The role of iron on the solid solution of $CaSiO_3$ and $MgSiO_3$ perovskites in the lower mantle

Tingting Xiao[1,2], Joshua M. R. Muir[1], Feiwu Zhang[1]*

[1]State Key Laboratory of Ore Deposit Geochemistry, Institute of Geochemistry, Chinese Academy of Sciences, Guiyang, 550081, China

[2]University of the Chinese Academy of Sciences, Beijing 100049, China

zhangfeiwu@mail.gyig.ac.cn

Abstract

The solid solution of $CaSiO_3$ and $MgSiO_3$ perovskites is an important control on the properties of the lower mantle but the effect of one of the largest defective elements (iron) on this solution is largely unknown. Using density functional theory (DFT), ferrous iron's influence on the reciprocal solubility of $MgSiO_3$ and $CaSiO_3$ perovskite (forming a single mixed perovskite phase) was calculated under pressures and temperatures of 25 - 125 GPa and 0 - 3000 K, respectively. Except in iron-rich conditions, iron preferentially partitions into the mixed perovskite phase over bridgmanite. This is a small effect (K_D~0.25-1), however, when compared to the partitioning of ferrous iron to ferropericlase which rules out phase mixing as a mechanism for creating iron-rich regions. Iron increases the miscibility of the two perovskite phases/reduces the temperature at which the two phases mix but this effect is highly nonlinear. We find that for pyrolytic mantle (Ca%=12.5 where Ca%=Ca/(Ca + Mg)) a perovskite iron concentration of ~13% leads to the lowest mixing temperature/highest miscibility. With this composition, 1% iron in the pyrolytic solution would lead to mixing at ~120 GPa along the geothermal gradient and 6.25% iron leads to mixing at ~115 GPa. At high iron concentrations Fe starts to impair miscibility, with 25% iron leading to mixing at ~120 GPa. Thus, in normal pyrolytic

mantle iron should induce a small amount of mixing near the D" layer. Extremely iron rich parts of the lower mantle such as potentially at the CMB and in ULVZs are, however, not a likely source of phase mixed perovskites due to the nonlinear effect of ferrous iron on phase mixing.

Keywords

Iron, $CaSiO_3$, $MgSiO_3$, miscibility, the lower mantle

1 Introduction

Earth's lower mantle, extending from 660 to 2890 km in depth, occupies nearly 75% of the mass of the bulk silicate Earth. Assuming that the lower mantle is pyrolytic and isochemically similar to the upper mantle, $MgSiO_3$ perovskite is considered to be the most abundant phase in the lower mantle, accounting for about 70% of the lower mantle, followed by ferropericlase (about 20%), and finally the least abundant phase is $CaSiO_3$-rich perovskite accounting for around 6-12% (Anderson et al. 1989; Oneill and Jeanloz 1990). Mg-rich silicate perovskite (Mg-pv) and $CaSiO_3$-rich perovskite (Ca-pv) are thus two of the main components of the lower mantle and subducted plates. Due to their similarity in chemical formula and structure, these two phases can dissolve into each other to some extent, forming a single $Mg_{1-x}Ca_X\ SiO_3$ phase. The solubility of Ca in Mg-pv and Mg in Ca-pv has been previously studied, and it is generally found that these two phases have very limited mutual solubility under lower mantle conditions (Armstrong et al. 2012; Fujino et al. 2004; Irifune et al. 2000; Irifune et al. 1989; Jung and Schmidt 2010; Muir and Zhang 2020; Tamai and Yagi 1989; Vitos et al. 2006). This limited solubility is speculated to be due to the large size difference between Mg^{2+} and Ca^{2+}, which could reduce miscibility (Jung and Schmidt 2010; Kesson et al. 1995; Vitos et al. 2006).

As the lower mantle is more Mg rich than Ca rich, we shall focus on the solubility of Ca in Mg-pv. Experimentally Irifune et al. (1989) found that the solid solubility of Ca in Mg-pv was limited to 2% or even lower at 25 GPa and ~1800 K. Armstrong et al. (2012) found that at 2000 K, the solubility of Ca in Mg-pv is less than 5 mol % at 30 GPa and at least 10 mol % at 55 GPa. With increasing pressure, the solubility thus increases. Theoretically Jung and Schmidt (2010) found that the solubility of Ca in Mg-pv was 0.5% at 25 GPa and 2000 K, but 5% at 25 GPa and 3000 K and Vitos et al. (2006) claimed that under the temperature and pressure conditions of the upper mantle and transition zone, the solid solubility of Ca in Mg-pv is 4-6%. Jung and Schmidt (2010) and Vitos et al. (2006) found that pressure decreased the solid solubility of Ca in Mg-pv in contrast with experimental findings (Armstrong et al. 2012). This was rectified by Muir and Zhang (2020) who found that the explicit inclusion of vibrational entropy caused pressure to increase miscibility. In this study they found that above the D'' pyrolytic compositions of Mg-pv and Ca-pv will not mix. Thus, all studies agree that pure Ca-pv and Mg-pv will not mix in pyrolytic compositions in lower mantle compositions except possibly in deep hot parts of the lower mantle.

Defect elements, such as Fe, Al, and Ti may, however, play important roles in the mixing of these phases. Armstrong et al. (2012) have clearly pointed out that the addition of titanium will enlarge the single phase domain of $MgSiO_3$-$CaSiO_3$. Muir and Zhang (2020) established a simple conceptual model to explore the influence of different impurities on the miscibility of Ca-pv and Mg-pv and found that large amounts of any defect element (>~1%) were required to significantly affect miscibility. Iron is the most prominent defect element in pyrolytic compositions and thus is a key candidate for potentially changing the dynamics of this phase mixing. In the lower mantle iron concentration in bridgmanite is around ~10% (Lin et al. 2018), and the iron concentration may be even higher near the Core Mantle Boundary (CMB). Fujino et al. (2004) explored the effect of iron on the perovskite two-phase mixing using laser heated DAC and TEM. They found that the solid solubility of Mg in Ca-pv was 4% at ~30 GPa and 1930 K but increased to ~18% at 30 GPa and 1800 K when around

9% iron was added which shows clearly that iron promotes miscibility at least to some degree. There was not enough P, T and Fe% points in that study, however, to explore systematically the effect of iron on the miscibility of the two perovskites. In this study, therefore, we conducted theoretical calculations to examine the effect of iron concentration, pressure (P) and temperature (T) on the mutual solubility of Ca-pv and Mg-pv in the conditions of the lower mantle.

2 Methodology

2.1 Computational Details

The simulations were carried out by VASP (Kresse and Furthmuller 1996a; Kresse and Furthmuller 1996b) using the projector-augmented-wave (PAW) method (Kresse and Joubert 1999) and the PBE formulation of GGA (Perdew et al. 1996; Perdew et al. 1997). In all calculations, the following PAW potentials were used: Core region cut-offs are 2.3 atomic units (a.u.) for calcium (core configuration $1s^2 2s^2 p^6$, $3s^2 3p^6 4s^2$ as valence), 1.9 a.u. for silicon (core configuration$1s^2 2s^2 2p^6$, $3s^2 3p^2$ as valence), 1.52 a.u. for oxygen (core configuration $1s^2$, $2s^2 2p^4$ as valence), 2.0 a.u. for magnesium (core configuration $1s^2 2s^2$, $2p^6 3s^2$ as valence) and 2.3 a.u. for iron (core configuration $1s^2 2s^2 2p^6 3s^2 3p^6$, $3d^7 4s^1$ as valence). Traditional DFT does not deal well with heavily correlated electrons such as the d electrons of transition metals, and so some kind of correction is needed to capture electron energy levels accurately. For this, we used the Hubbard U approach (where an additional localized energy penalty is introduced for intra-atomic interactions), and we used the rotationally invariant formulation of GGA+U introduced by Dudarev et al. (1998). The empirical value of U_{eff} (U-J) was set to be 2.5 eV.

A unit cell of 40 atoms was used in static calculations and one with 80 atoms (2x2x1) in Molecular dynamics (MD) simulations. In our calculations, $Mg_xFe_{1-x}SiO_3$ and $Mg_{1-x-y}Ca_yFe_xSiO_3$ were modelled with an orthorhombic (pbnm) unit cell, for $Mg_{1-x-y}Ca_yFe_xSiO_3$ i4mcm and pm3m structures were found to be less stable at all P and T conditions. For

$CaSiO_3$ both i4mcm and pm3m phases were modelled with pm3m favoured at high temperatures. Calculations were done at 25, 75 and 125 GPa (all pressures are uncorrected) and at 0, 1000, 2000 and 3000 K. Static simulations (~0 K) were calculated with a (3x5x5) k-point mesh, and molecular dynamics runs were conducted at the gamma point only. Both static and MD calculations had an energy cutoff of 500 eV and were converged to within 10^{-5}eV.

2.2 Mixing Thermodynamics

In order to find the solubility of $CaSiO_3$ and (Mg, Fe) SiO_3, we examined the following reaction:

$$xCaSiO_3 + Mg_{1-y}Fe_ySiO_3 \rightarrow Ca_xFe_yMg_{1-x-y}SiO_3 + xMgSiO_3$$

Reaction 1

The iron is placed in Mg-pv before mixing is simulated. Although some iron must thermodynamically enter into Ca-pv as shown in the text this amount is generally negligible and can be ignored. To determine mixing we calculate the free energy of Reaction 1 using

$$G_{Mix} = H_{Mix} - TS_{Mix}$$ Equation 1

where G_{Mix} = 0 represents the mixing boundary and mixing occurs when it is negative. T_{Mix} is the mixing temperature defined as the T which makes G_{Mix} = 0 (*ie.* the solvus temperature). H_{Mix} is the mixing enthalpy. Determining S_{Mix} (the mixing entropy) is complex; in our case we have defined it as the sum of two parts- configurational and vibrational entropies.

For the configurational entropy, for each specific calcium and iron content in the unit cell we calculated the relative enthalpy of different configurations of Fe, Ca and Mg where a configuration is the arrangement of Fe, Ca and Mg across the A lattice sites. We then used this equation (Gibb's entropy equation):

$$S_{Config} = -k_b \sum_i \frac{1}{\sum_i e^{\frac{-E_i}{kbT}}} e^{\frac{-E_i}{kbT}} ln \frac{1}{\sum_i e^{\frac{-E_i}{kbT}}} e^{\frac{-E_i}{kbT}}$$ Equation 2

where k_b is Boltzmann's constant, T is temperature and E_i is the relative energy of each configuration. Strictly speaking S_{config} should be determined with the relative energy of each configuration including their high temperature components. Practically the difference in phonons between different configurations should be small particularly if their relative enthalpy is small which is indicative of no large structural rearrangements. As outlined in the text we find enthalpy differences between different arrangements to not be large. Thus, we shall use the relative enthalpy in each case when calculating Equation 2. The number of theoretical arrangements in each case is $Z = \frac{N!}{N_{Mg}!*N_{Ca}!*N_{Fe}!}$ (N is the sum of Mg, Ca and Fe). By symmetry these can be reduced to 1/4 Z. We calculated all degenerate arrangements for x = 0 / 0.125 / 0.25 / 0.375 / 0.5 / 0.625 / 0.75 / 0.825 and y=0 / 0.125 / 0.25 in Reaction 1 and then applied Equation 2. Thus, we cover all possible arrangements of Fe, Ca and Mg in our 40 atom unit cells when these atoms are confined to relaxed A lattice sites. In addition, we calculate the "perfect" entropy which is the entropy if all arrangements had the same energy- the Boltzmann entropy. This is done via $S_{config} = k_b \ln Z$ where Z is the total number of arrangements of all atoms as outlined above. We found that the difference between the two calculation methods is very small as outlined in the paper. Therefore, our configuration entropy for mixing in this study is calculated by the formula $S_{config} = k_b \ln Z$.

For vibrational entropy (S_{vib}), we obtain the velocity autocorrelation function through molecular dynamics calculations. The vibrational entropy is then determined by:

$$S(\nu) = \frac{2}{k_b T} \sum_{i=1}^{N} \sum_{k=1}^{3} m_a s_a^k \qquad \text{Equation 3}$$

$$S_{Vib} = k_b \int_0^{\infty} S(v) dV \qquad \text{Equation 4}$$

where N is the number of atoms in the system, m_a is the mass of atom a, s_a^k is the spectral density of atom a in the direction k (x=1, y=2, z=3) and V is the velocity.

3 Result & Discussion

3.1 Compositions

In this work, we examine how varying the Ca and the Fe content of bridgmanite and Calcium silicate perovskite (Ca-pv) mixtures varies their solubilities. We shall thus define two terms Ca% which is Ca / (Mg + Ca + Fe) x 100%, and Fe%, which is Fe / (Mg + Ca + Fe) x 100%. The calcium content varies in different compositions that can occur in the lower mantle. The Ca% of mid-ocean ridge basalt (MORB) is between 30-60% (Hirose 2002; Hirose et al. 2005; Ricolleau et al. 2010), of harzburgitic compositions 1-3% (Michael and Bonatti 1985; Ringwood 1991) and of pyrolytic compositions around 7-13% (Kesson et al. 1998; Mattern et al. 2005; Ringwood 1991). Iron in the lower mantle can have multiple oxidation states (primarily 2^+ and 3^+) and structural sites (A and B) (Gialampouki et al. 2018; Muir and Brodholt 2020; Wang et al. 2019). As we are interested in finding the effect of iron on A site mixing of Ca and Mg, we shall focus on ferrous iron at the A site. This is likely also the predominant oxidation state of iron across the lower mantle in the absence of Aluminum (Wang et al. 2019). The iron content of Bridgmanite in the lower mantle is about 10% (Lin et al. 2018) but maybe lower or higher in some regions and so we shall study iron concentrations of 0-25%. Ferrous iron of Bridgmanite is in a state of high spin (Shim et al. 2017; Shukla et al. 2015; Xu et al. 2015) under mantle pressures and temperatures and so all of our calculations will have iron fixed to the high spin state.

3.2 Fe Partitioning

It is important to know into which of the three phases, Ca-pv, Mg-pv and the mixed phase, that iron likes to partition. The partitioning coefficient of Fe between $MgSiO_3$ and $CaSiO_3$ is defined as ($K_{D1}^{Fe} = X_{Fe}^{Mg-pv} / X_{Fe}^{Ca-pv}$) (Table 1), and between $Mg_{1-x}Ca_xSiO_3$ and $MgSiO_3$ is defined as ($K_{D2}^{Fe} = X_{Fe}^{(Mg_{1-x}Ca_x)SiO_3} / X_{Fe}^{Mg-pv}$) (Table 2). Between Mg-pv and Ca-pv we find that Fe has strongly preferential partitioning into $MgSiO_3$. Between Mg-pv and the mixed phase we find that except for very large amounts of iron at low pressures (where

mixing is not expected to occur), iron always favors the mixed phase over Mg-pv and this preference increases with pressure. This preference is not particularly strong with all K_D values being above 0.25 except with extreme iron contents or in a basaltic mixture. The amount of iron in the system has an effect on the partitioning but it this small as shown in Figure 1. In no cases at high pressure (where mixing is likely to occur) does iron favor bridgmanite over the mixed phase.

In the lower mantle a third phase is present, that of ferropericlase. Iron could potentially partition from bridgmanite either to ferropericlase or to the mixed phase. Muir and Brodholt (2016) claimed that there is a strong partitioning of iron from bridgmanite to ferropericlase with a K_D of ~0.32 at 30 GPa dropping to ~0.06 at 120 GPa at 2000 K and dropping further with increased temperature. This is a much stronger preference of iron into ferropericlase than is seen with the mixed phase and so the preference of ferrous iron at deep mantle pressures and temperatures where mixing occurs (see Figure 5) is ferropericlase > the mixed phase > bridgmanite in that order. Thus, the formation of a perovskite mixed phase does not outcompete ferropericlase as an iron-sink and should not substantially alter the distribution of iron in the deep lower mantle. Our concentrations of iron in the rest of the paper shall refer to the concentration of ferrous iron in the perovskite phases (bridgmanite and the mixed phase). In a real lower mantle with ferropericlase this concentration will be lower than the concentration of iron in the system and could be up to 20 times lower as we approach the CMB (Muir and Brodholt (2016)).

3.3 Effect of Iron on Mixing Energies

H_{Mix}

We determined the effect of iron on the mixing enthalpy (H_{Mix}) using static DFT calculations as shown in Figure 2. The mixing enthalpy has a nonlinear trend with iron content. H_{Mix} is always positive showing that Ca-pv and Mg-pv are naturally immiscible and temperature is required to mix them. With increasing pressure H_{Mix} increases which will lead

to less mixing. Iron in general decreases H_{Mix} and thus promotes phase mixing. Initially with an increasing concentration of iron, H_{Mix} decreases but then after a point H_{Mix} increases with increasing Fe concentration. The reason for this nonlinearity can be seen in Figure S1, which plots the change in energy of $Mg_{1-x}Fe_xSiO_3$ and $Mg_{1-x-y}Fe_{1-x}Ca_ySiO_3$ as a function of iron content. Replacing a Mg atom with a Fe atom has a similar effect on the enthalpies of the mixed phase and Mg-pv as both structures are extremely similar. Thus, the effect of iron on the enthalpy difference between these two systems is highly sensitive to small deviations from linearity. Such deviations grow larger as the iron concentration increases and both mixed and unmixed structures begin to transition to an iron-rich member which has significant structural and energetic differences to the Mg-rich end-member. While the effect of defects on properties like enthalpy are often linear with concentration, defects are usually present in much smaller concentrations and at higher concentrations there are significant defect-defect interactions which can deviate this behavior. It is important to stress that all configurations of iron were tested for a set Fe% and Ca% and the lowest energy used in all cases so this nonlinear trend is not an artefact of the favored arrangement of iron in these systems changing with concentration. The energy of different iron configurations with a fixed composition can be up to 0.15 eV/f.u. and so is similar to the energy difference between unmixed and mixed phases.

S_{Config}

We examined the effect of different iron arrangements, as explained in the method, to estimate the effect of iron on configurational entropy (S_{Config}). In a perfect system (where all arrangements of atoms are energetically equivalent) the presence of iron does not cause an increase to S_{Config}. This is because iron exists on the A site where mixing between Mg and Ca occurs in the perfect system and because iron is primarily partitioned to a single phase before mixing. As shown in Table S1, the configurational entropy of iron, Mg and Ca is near the perfect Boltzmann entropy limit. At all conditions, the difference between a perfect configurational entropy and our actual configurational entropy is < ~ 4 meV/atom. This is a

very small energy term and is much smaller than the H_{Mix} term. This suggests that all arrangements Mg, Fe and Ca on the A sites in both Mg-pv and the mixed phase are effectively equivalent and that iron does not cause large structural rearrangements in the Mg-pv or the mixed phase. Considering a system with 12.5% Fe and 12.5% Ca changing between perfect and non-perfect entropy changes the mixing temperature by ~50 K. Thus, the primary effect on iron on mixing should be enthalpic and effect of iron on S_{config} can be largely ignored.

S_{Vib}

Vibrational entropy (S_{Vib}) depends on long-range phonons and is likely unaffected by small additions but could be strongly affected by defects present in large quantities like Fe. S_{Vib} is essential to calculating mixing parameters of these systems (Muir and Zhang 2020) but ΔS_{Vib}-Fe (the change caused to S_{Vib} by iron) is not. Iron makes no large structural rearrangements to the system as indicated by S_{config} and thus likely also has small effects on long range entropy. As shown in Table 3, the change in the vibrational entropy term from replacing a Mg atom with an iron atom is extremely small particularly at high pressures where mixing occurs. Therefore, in this work we shall include S_{Vib} but ignore the effects of ΔS_{vib}-Fe.

3.4 Mixing

In Figure 3, we plot the T_{mix} of a 1:7 (pyrolytic) mixture of Ca-pv and Bridgmanite as a function of iron at pressures of 25, 75 and 125 GPa. When iron is added into the system, initially the mixing temperature decreases by about 80 K per 1% Fe. This T_{mix} decrease in a pyrolytic mixture is not universal with concentration, however. At ~13% iron we see a maximum decrease in T_{mix} and beyond this increasing the iron concentration causes T_{mix} to rise. As shown in Figure 2 Fe decreases in H_{Mix} are largest at ~13% and increase on either side and these nonlinear H_{mix} effects are the origin of this non-linear T_{mix} behaviour. This

means that while a small amount of iron (6.25%) causes a T_{mix} decrease of 500 K a large amount of iron (25%) causes a decrease in T_{mix} of less than 100 K.

Unlike the behavior of the pyrolytic mixture, in a 1:1 mixture of Ca-pv and Mg-pv (Ca%=50, basaltic) T_{mix} decreases with iron concentration continually up until 25%. A likely explanation for these differing behaviors of pyrolytic and basaltic compositions is due to iron partitioning preferences. The iron partition coefficient (K_{D1}^{Fe}) between $CaSiO_3$ and $MgSiO_3$ is very large, with strong partitioning of Fe into the Mg end-member. The iron partition coefficient (K_{D2}^{Fe}) between bridgmanite and the mixed phase is smaller and closer to 1, particularly at lower pressures. Thus, there is a strong dislike of Fe going into Ca sites rather than Mg sites which makes sense as Fe^{2+} is much closer in size to Mg^{2+} than Ca^{2+} (~78/72/100 pm respectively). At low iron concentrations iron partitions into the mixed phase and thus reduces the mixing temperature. As iron concentration increases relative to Ca concentration increasingly iron will partition into the Mg-end member and not take part in the miscibility process. Thus, it will cost energy to put the surplus iron back into the mixture (T_{mix} increase). When Ca% is 12.5% (pyrolytic mixture), the iron-driven two-phase solid solution T_{mix} minimum is around 13% Fe, when Ca% is 50% (basaltic mixture) this T_{mix} minimum increases to ~30% Fe which has not been plotted in the Figure 3.

In the deep lower mantle, the $CaSiO_3$ and $MgSiO_3$ two-phase mixing temperature at 125 GPa is about 2550 K in the Fe free system for both a pyrolytic mixture (Ca%=12.5) and a basaltic mixture (Ca%=50) (Figure 4). With the introduction of 6.25%/12.5% iron the mixture temperatures reduce to ~2280 K/~2180 K for the pyrolytic mixture and ~2290 K/2040 K for the basaltic mixture. With a large amount of iron (25% Fe) the mixing temperature is very different in pyrolytic (~2520 K) and basaltic (~1850 K) mixtures for the reasons discussed above. Direct comparison with Fujino *et al.* (2004) is difficult due to the high levels of Fe involved in that study (with Fe nearly equivalent to Mg) and its focus on the Ca-pv side of the solubility diagram. As demonstrated above the behavior of high iron concentrations is not easy to predict and the concentrations of iron in that study are beyond the scope of our

calculations. Regardless our study is consistent with the findings of Fujino et al. (2004) in that iron can promote the miscibility of two phases.

Figure 5 presents the mixing temperature of a pyrolytic mixture (Ca%=12.5) as a function of depth and iron concentration. Regardless of the amount of iron no mixing is seen at the top of lower mantle. With the amount of iron that causes the maximum mixing (~13%) perovskite phase mixing can be seen to occur at ~70 GPa in the hottest parts of the mantle. As the iron concentration increases or decreases or the mantle cools then mixing occurs at deeper parts of the mantle. 13% would be an extremely iron rich part of the mantle, especially when considering the effect of ferropericlase, and more reasonable iron concentrations lie between 0-6.25%. With these iron concentrations and the "standard" geotherm mixing is found to occur between 115-125 GPa depending upon the iron concentration. Thus, in pyrolytic mantle iron causes only very small changes to the depth at which phase mixing occurs and is not a large control on this process. Similar observations can be made with the basaltic phase (Figure S2) but in this case the higher Ca% means no phase mixing is observed under any conditions. As shown in Figure 4 the Ca% of the pyrolytic mixture has little effect on the mixing temperature across the observed range of pyrolite and at most causes T_{mix} by vary by ~50 K.

Iron-rich regions present an interesting case. Various regions, particularly those near the CMB, have been speculated to be iron rich and these could present quite different behaviour from the rest of the mantle. We find however that large amounts of iron decrease the stability of the mixed phase and do not promote its formation. Thus, these regions would not have different phase characteristics from the rest of the more iron-poor mantle. The potential formation of a mixed phase also does not provide a mechanism for forming iron rich regions. Strong partitioning of iron from bridgmanite to the mixed phase could provide a physical mechanism for dynamically separating iron from the overall mantle across the physical barrier of a phase transition but the partitioning coefficient is small (Table 2) and moves closer to 1 with increasing iron (Figure 1).

So far, we have considered only univariant mixing but the introduction of iron will lead to a phase loop. Calculating the exact dimensions of this phase loop is challenging. The similar trends of formation enthalpies vs Fe% for Mg-pv and the mixed phase (Figure S1), and their highly variable relationship to each other means that constraining the phase loop requires very high accuracy in both the number of Fe concentrations that are measured and the precision of those points. This is potentially important future work but the phase loop is unlikely to be large or important simply due to the partitioning of Fe between Mg-pv and the mixed phase being near 1. A wide phase loop would require strong partitioning of the iron to either Mg-pv or the mixed phase. Using a common tangent method, we calculate that at 125 GPa the width of the phase loop is < 200 K at 6.25% Fe and < 50 K at 12.5% Fe (both with Ca%=10), but there could be large inaccuracies in this method. Regardless it is difficult to propagate a width phase loop in Fe space for the perovskite mixing reaction due to their close partitioning values.

Finally, we consider the effect of other elements. The two other major components we expect to be important are Ferric iron and Aluminum. While ferrous iron is expected to be dominant over ferric iron (Xu et al. 2015) the presence of Aluminum can make Fe^{3+}-Al^{3+} and Al could also affect mixing dynamics. The effect of these elements was studied with a simple enthalpic model in Muir and Zhang (2020) where it was concluded that Al raises the mixing temperature and Fe^{3+}-Al^{3+} causes the mixing temperature to remain largely static. While this was a simplistic model it correctly predicts the trends seen for Fe^{2+} at low Fe concentrations. It did not predict the high concentration effects of Fe^{2+} on mixing seen in this study because it assumed a linear effect of Fe on enthalpy which is not the case (Figure 2). Thus, this model likely captures the broad trend of Ferric iron and aluminum in that they have little effect or slightly raise the mixing temperature. Thus, these elements further reduce the miscibility of Ca-pv and Mg-pv and adding in Fe-Al or Al to our model likely will not lead to phase mixing. Therefore, our predictions here represent the most favorable conditions for mixing in the

lower mantle and adding in Al and/or converting iron to Ferric iron will not lead to increased mixing.

4 Conclusion

The effect of iron on Ca-pv and Mg-pv perovskite phase mixing also been investigated in this study. Iron reduces the mixing temperature/increases miscibility but in highly non-linear ways. Low iron contents promote the mixing of these two phases but only to a small degree whereas high iron contents have very little effect on the miscibility of these phases and can even hinder mixing. We find that Ca-pv and Mg-pv exist as independent phases in the lower mantle but starting at 75 GPa in iron-rich hot mantle they can form a single phase. As iron content decreases or the mantle cools the pressure of this transition deepens to around 120 GPa for a mantle at normal temperatures with a small amount of iron (~1% Fe in the perovskite). There is weak partitioning of iron from bridgmanite to the mixed phase but this is less favourable than partitioning Fe from bridgmanite to MgO and thus is not expected to have strong dynamical consequences.

5 Acknowledgement

This work was supported by National Natural Science Foundation of China (41773057), with computational re-sources from Computer Simulation Labs of IGGCAS, the National Supercomputer Centers in Shenzhen and Beijing, China.

6 References

Anderson OL, Isaak DG, Yamamoto S (1989) Anharmonicity and the equation of state for gold Journal of Applied Physics 65:1534-1543 doi:10.1063/1.342969

Armstrong LS, Walter MJ, Tuff JR, Lord OT, Lennie AR, Kleppe AK, Clark SM (2012) Perovskite Phase Relations in the System CaO-MgO-TiO_2-SiO_2 and Implications for Deep Mantle Lithologies Journal of Petrology 53:611-635 doi:10.1093/petrology/egr073

Dudarev SL, Botton GA, Savrasov SY, Humphreys CJ, Sutton AP (1998) Electron-energy-loss spectra and the structural stability of nickel oxide: An LSDA+U study Physical Review B

57:1505-1509 doi:DOI 10.1103/PhysRevB.57.1505
Fujino K, Sasaki Y, Komori T, Ogawa H, Miyajima N, Sata N, Yagi T (2004) Approach to the mineralogy of the lower mantle by a combined method of a laser-heated diamond anvil cell experiment and analytical electron microscopy Physics of the Earth and Planetary Interiors 143-144:215-221 doi:10.1016/j.pepi.2003.11.013
Gialampouki MA, Xu S, Morgan D (2018) Iron valence and partitioning between post-perovskite and ferropericlase in the Earth's lowermost mantle Physics of the Earth and Planetary Interiors 282:110-116 doi:10.1016/j.pepi.2018.06.005
Hirose K (2002) Phase transitions in pyrolitic mantle around 670-km depth: Implications for upwelling of plumes from the lower mantle Journal of Geophysical Research: Solid Earth 107:ECV 3-1-ECV 3-13 doi:10.1029/2001jb000597
Hirose K, Takafuji N, Sata N, Ohishi Y (2005) Phase transition and density of subducted MORB crust in the lower mantle Earth and Planetary Science Letters 237:239-251 doi:10.1016/j.epsl.2005.06.035
Irifune T, Miyashita M, Inoue T, Ando J, Funakoshi K, Utsumi W (2000) High-pressure phase transformation in $CaMgSi_2O_6$and implications for origin of ultra-deep diamond inclusions Geophysical Research Letters 27:3541-3544 doi:10.1029/2000gl012105
Irifune T, Susaki J, Yagi T, Sawamoto H (1989) Phase-Transformations in Diopside $CaMgSi_2O_6$ at Pressures up to 25-Gpa Geophysical Research Letters 16:187-190 doi:DOI 10.1029/GL016i002p00187
Jung DY, Schmidt MW (2010) Solid solution behaviour of $CaSiO_3$ and $MgSiO_3$ perovskites Physics and Chemistry of Minerals 38:311-319 doi:10.1007/s00269-010-0405-0
Kesson SE, Fitz Gerald JD, Shelley JM (1998) Mineralogy and dynamics of a pyrolite lower mantle Nature 393:252-255 doi:Doi 10.1038/30466
Kesson SE, Fitz Gerald JD, Shelley JMG, Withers RL (1995) Phase-Relations, Structure and Crystal-Chemistry of Some Aluminous Silicate Perovskites Earth and Planetary Science Letters 134:187-201 doi:Doi 10.1016/0012-821x(95)00112-P
Kresse G, Furthmuller J (1996a) Efficiency of ab-initio total energy calculations for metals and semiconductors using a plane-wave basis set Comp Mater Sci 6:15-50 doi:Doi 10.1016/0927-0256(96)00008-0
Kresse G, Furthmuller J (1996b) Efficient iterative schemes for ab initio total-energy calculations using a plane-wave basis set Physical Review B 54:11169-11186 doi:DOI 10.1103/PhysRevB.54.11169
Kresse G, Joubert D (1999) From ultrasoft pseudopotentials to the projector augmented-wave method Physical Review B 59:1758-1775 doi:DOI 10.1103/PhysRevB.59.1758
Lin JF, Mao Z, Yang J, Fu S (2018) Elasticity of lower-mantle bridgmanite Nature 564:E18-E26 doi:10.1038/s41586-018-0741-7
Mattern E, Matas J, Ricard Y, Bass J (2005) Lower mantle composition and temperature from mineral physics and thermodynamic modelling Geophysical Journal International 160:973-990 doi:10.1111/j.1365-246X.2004.02549.x
Michael PJ, Bonatti E (1985) Peridotite Composition from the North-Atlantic - Regional and Tectonic Variations and Implications for Partial Melting Earth and Planetary Science Letters 73:91-104 doi:Doi 10.1016/0012-821x(85)90037-8
Muir JMR, Brodholt JP (2016) Ferrous iron partitioning in the lower mantle Physics of the Earth and Planetary Interiors 257:12-17 doi:10.1016/j.pepi.2016.05.008
Muir JMR, Brodholt JP (2020) Ferric iron in bridgmanite and implications for ULVZs Physics of the Earth and Planetary Interiors 306 doi:10.1016/j.pepi.2020.106505
Muir JMR, Zhang F (2020) The miscibility of Calcium Silicate Perovskite and Bridgmanite: A single phase perovskite in hot, iron-rich regions Submitted Preprint:https://doi.org/10.31223/X56309
Ohtani E, Yuan L, Ohira I, Shatskiy A, Litasov K (2018) Fate of water transported into the deep mantle by slab subduction J Asian Earth Sci 167:2-10 doi:10.1016/j.jseaes.2018.04.024
Oneill B, Jeanloz R (1990) Experimental Petrology of the Lower Mantle - a Natural Peridotite Taken to 54 Gpa Geophysical Research Letters 17:1477-1480 doi:DOI 10.1029/GL017i010p01477
Perdew JP, Burke K, Ernzerhof M (1996) Generalized gradient approximation made simple Phys Rev Lett 77:3865-3868 doi:DOI 10.1103/PhysRevLett.77.3865

Perdew JP, Burke K, Ernzerhof M (1997) Generalized gradient approximation made simple (vol 77, pg 3865, 1996) Phys Rev Lett 78:1396-1396 doi:DOI 10.1103/PhysRevLett.78.1396

Ricolleau A et al. (2010) Phase relations and equation of state of a natural MORB: Implications for the density profile of subducted oceanic crust in the Earth's lower mantle Journal of Geophysical Research 115 doi:10.1029/2009jb006709

Ringwood AE (1991) Phase-Transformations and Their Bearing on the Constitution and Dynamics of the Mantle Geochim Cosmochim Ac 55:2083-2110 doi:Doi 10.1016/0016-7037(91)90090-R

Shim SH et al. (2017) Stability of ferrous-iron-rich bridgmanite under reducing midmantle conditions Proc Natl Acad Sci U S A 114:6468-6473 doi:10.1073/pnas.1614036114

Shukla G, Wu ZQ, Hsu H, Floris A, Cococcioni M, Wentzcovitch RM (2015) Thermoelasticity of Fe^{2+}-bearing bridgmanite Geophysical Research Letters 42:1741-1749 doi:10.1002/2014gl062888

Tamai H, Yagi T (1989) High-Pressure and High-Temperature Phase-Relations in $CaSiO_3$ and $CaMgSi_2O_6$ and Elasticity of Perovskite-Type $CaSiO_3$ Physics of the Earth and Planetary Interiors 54:370-377 doi:Doi 10.1016/0031-9201(89)90254-9

Vitos L, Magyari-Köpe B, Ahuja R, Kollár J, Grimvall G, Johansson B (2006) Phase transformations between garnet and perovskite phases in the Earth's mantle: A theoretical study Physics of the Earth and Planetary Interiors 156:108-116 doi:10.1016/j.pepi.2006.02.004

Wang XL, Tsuchiya T, Zeng Z (2019) Effects of Fe and Al incorporations on the bridgmanite-postperovskite coexistence domain C R Geosci 351:141-146 doi:10.1016/j.crte.2018.10.003

Xu S, Shim S-H, Morgan D (2015) Origin of Fe^{3+} in Fe-containing, Al-free mantle silicate perovskite Earth and Planetary Science Letters 409:319-328 doi:10.1016/j.epsl.2014.11.006

Figure captions

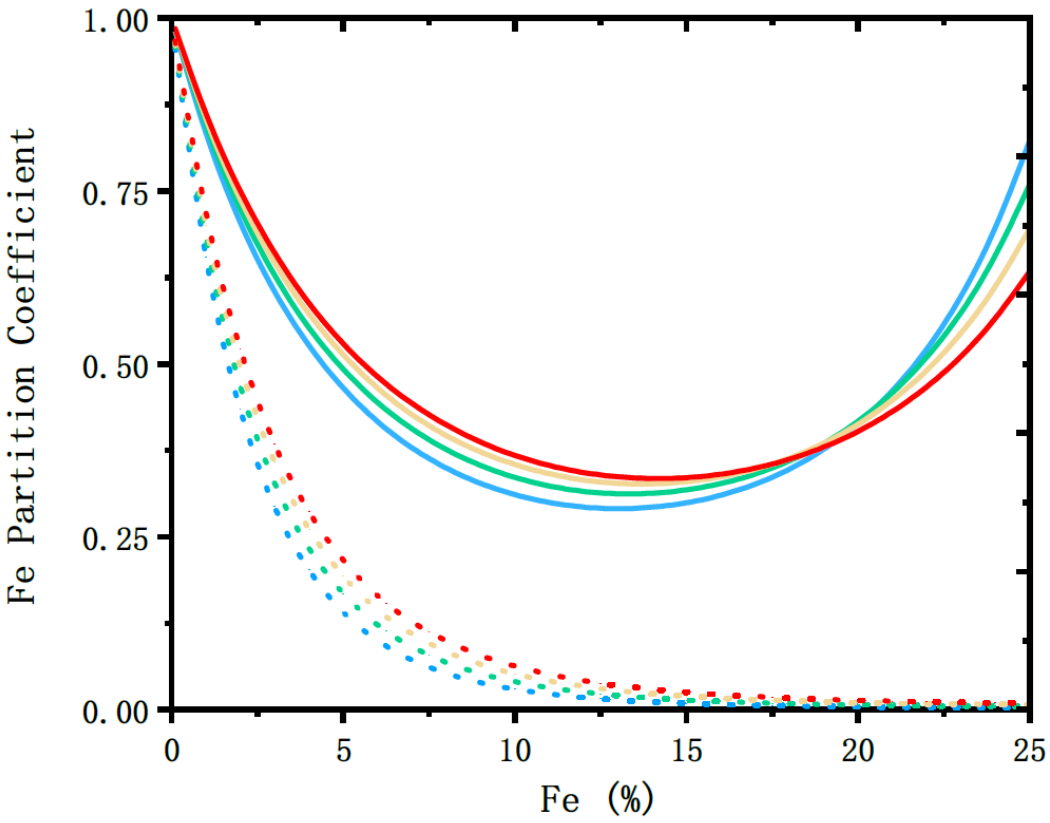

Figure 1

Plot of the partitioning coefficient of Fe between $Mg_{1-x}Ca_xSiO_3$ x=0.125(solid line)/0.5(dashed line) and $MgSiO_3$ ($K_{D2}^{Fe} = X_{Fe}^{(Mg_{1-x}Ca_x)SiO_3} / X_{Fe}^{Mg-pv}$) at 125 GPa and 2250 - 3000 K. Blue line represents 2250 K, green: 2500 K, yellow: 2750 K and red: 3000 K

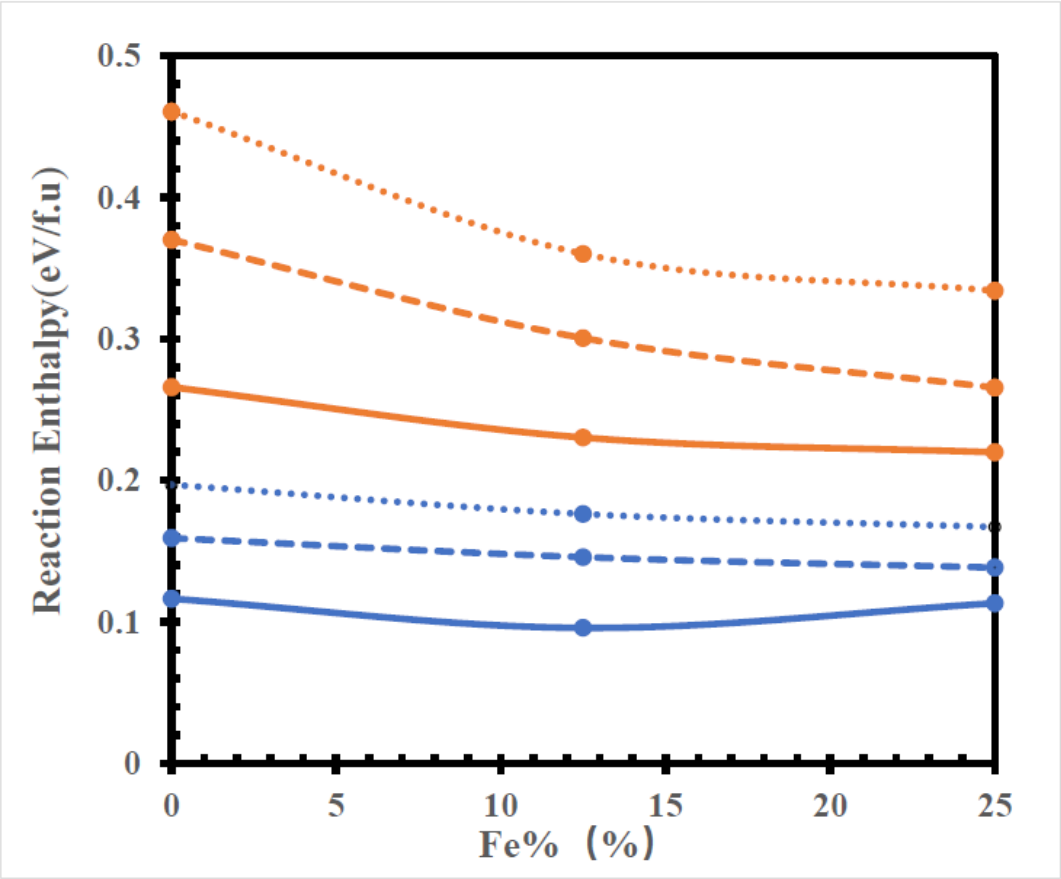

Figure 2 Reaction enthalpies (H_{mix}) of chemical reaction 1 with x=12.5% (blue line) and 50% (orange line), as the function of iron contents at three pressures of 25 GPa (solid line), 75 GPa (dashed line), and 125 GPa (dotted line) respectively

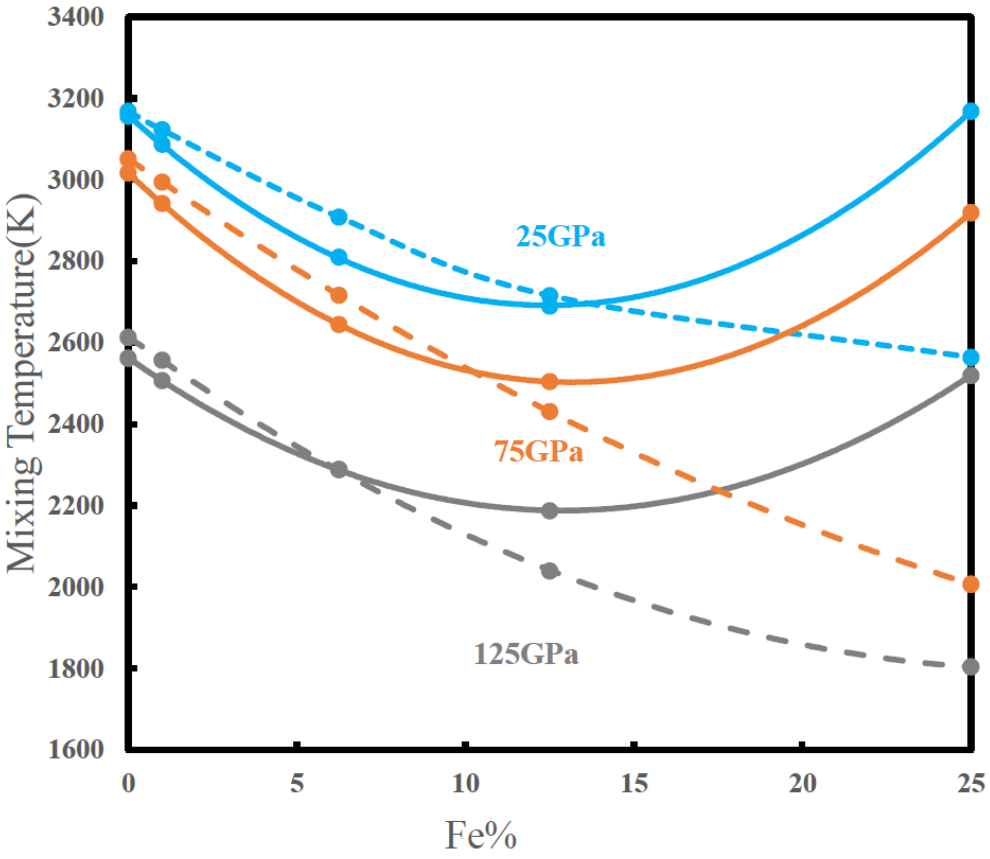

Figure 3 Plot of the mixing temperature (T_{mix}) for Ca: Mg = 1:7 (solid line) and 1:1 (dashed line) mixtures of Ca-pv and Bridgmanite phases at the pressure of 25 GPa (blue line), 75 GPa (orange line) and 125 GPa (grey line) as the function of iron concentration

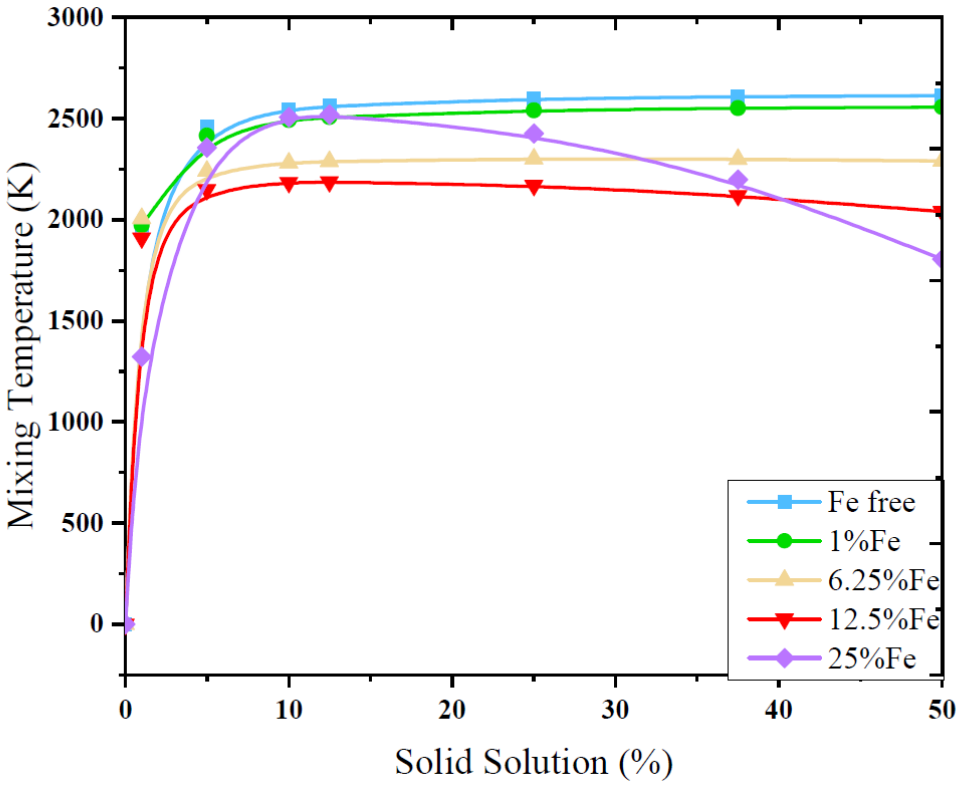

Figure 4 Solid solubility of Ca (Ca%) in Bridgmanite as a function of mixing temperature at 125 GPa. The blue line represents Fe free, green: 1% Fe, yellow: 6.25% Fe, red: 12.5% Fe and purple 25% iron

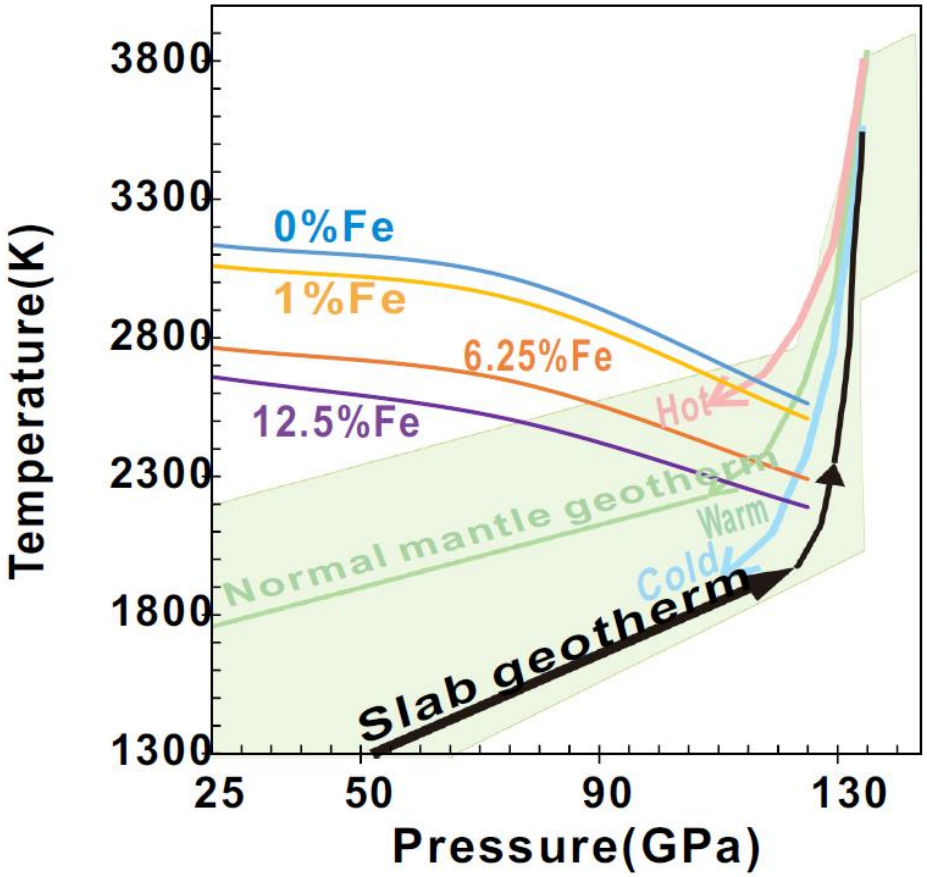

Figure 5 Plot of the mixing temperature (T_{mix}) for Ca: Mg =1:7 mixture of Ca-pv and Bridgmanite phases in Fe free (blue line), 1% Fe (yellow line), 6.25% Fe (orange line) and 12.5% Fe (purple line) bearing systems. the normal mantle geothermal gradient and the cold subduction slab geothermal is also presented for guidance (Ohtani et al. 2018)

Table 1 The partitioning coefficient of Fe between $MgSiO_3$ and $CaSiO_3$ ($K_{D1}^{Fe} = X_{Fe}^{Mg-pv} / X_{Fe}^{Ca-pv}$) at 25 - 125 GPa and 1000 - 3000 K.

	1000 K	2000 K	3000 K
25 GPa	3.116	1.765	1.461
75 GPa	6.548	2.559	1.871
125 GPa	21.815	4.671	2.794

Table 2 The partitioning coefficient of Fe between $Mg_{1-x}Ca_xSiO_3$ (x=0.125/0.5) and $MgSiO_3$ ($K_{D2}^{Fe} = X_{Fe}^{(Mg_{1-x}Ca_x)SiO_3} / X_{Fe}^{Mg-pv}$) at 25 - 125 GPa and 2000 - 3000 K.

	K_{D2} (x=0.125)					
	2000 K		2500 K		3000 K	
	6.25%Fe	25%Fe	6.25%Fe	25%Fe	6.25%Fe	25%Fe
25 GPa	0.634	4.485	0.694	3.322	0.738	2.719
75 GPa	0.446	0.809	0.524	0.844	0.583	0.868
125 GPa	0.372	0.882	0.434	0.759	0.471	0.633
	K_{D2} (x=0.5)					
	2000 K		2500 K		3000 K	
	6.25%Fe	25%Fe	6.25%Fe	25%Fe	6.25%Fe	25%Fe
25 GPa	0.407	0.227	0.487	0.305	0.549	0.372
75 GPa	0.190	0.006	0.264	0.016	0.330	0.031
125 GPa	0.070	0.002	0.114	0.005	0.155	0.010

Table 3: Value of delta S_{vib}-Fe (the change in the vibrational entropy term from replacing a Mg atom with an Fe atom) for adding 1 iron to 80-atom bridgmanite (Fe%=6.25) and the mixed phase with Ca%=50.

delta S_{vib}-Fe (meV/atom)				
Pressure	Temperature	bridgmanite	mixed phase	difference
25 GPa	1000 K	-2.6	-0.3	2.3
	2000 K	-2.2	-0.1	2.1
	3000 K	-1.6	-0.3	1.3
125 GPa	1000 K	-4.1	-4	0.1
	2000 K	-4	-3.9	0.1
	3000 K	-3.8	-4.4	-0.6

Table S1 List of S_{Config} (in $meVK^{-1}unit^{-1}$,) changes upon mixing Ca-pv and bdg for various Ca% of and various Fe% values at different pressures (25,75and 125 GPa) as determined by the method presented in the methods. different phases are presented as is a hypothetical "perfect" phase where all configurations of Fe:Si and Ca:Mg have the same energy.

		0	12.5	25	37.5	50	62.5	75	100
	Fe free	0	0.000179	0.000275	0.000342	0.000345	0.000346	0.000254	0
25GPa	12.5% Fe	0	0.000346	0.000441	0.000485	0.000485	0.000379	0.000347	0
	25% Fe	0	0.000441	0.000520	0.000525	0.000520	0.000442	0.000000	0
	Fe free	0	0.000179	0.000269	0.000335	0.000326	0.000347	0.000255	0
75GPa	12.5% Fe	0	0.000345	0.000439	0.000482	0.000485	0.000424	0.000345	0
	25% Fe	0	0.000440	0.000519	0.000544	0.000520	0.000442	0.000000	0
	Fe free	0	0.000179	0.000264	0.000327	0.000309	0.000346	0.000262	0
125GPa	12.5% Fe	0	0.000344	0.000436	0.000477	0.000485	0.000424	0.000347	0
	25% Fe	0	0.000440	0.000519	0.000542	0.000520	0.000441	0.000000	0
Perfect	Fe free	0	0.000179	0.000287	0.000347	0.000366	0.000347	0.000287	0
Perfect	12.5% Fe	0	0.000347	0.000442	0.000486	0.000486	0.000442	0.000347	0
Perfect	25% Fe	0	0.000442	0.000521	0.000545	0.000521	0.000442	0.000000	0

Table S2 Change in H_{mix} (in eV) upon mixing a mixture of Ca-pv and bdg with various values of Ca% and Fe%. at different pressures (25,75and 125 GPa).

			enthalpy of mixing(ev)				
		12.5%Ca	25%Ca	37.5%Ca	50%Ca	62.5%Ca	75%Ca
	Fe free	0.9308	1.6612	2.0161	2.1268	2.1247	1.8347
25GPa	12.5% Fe	**0.7659**	**1.3165**	1.6789	**1.8419**	1.8018	**1.5636**
	25% Fe	**0.9051**	1.5877	**1.8721**	1.7584	**1.2467**	0.3368
	Fe free	1.2733	2.1968	2.7553	2.9602	2.8229	2.3282
75GPa	12.5% Fe	**1.1658**	**1.8452**	2.2629	2.4042	2.2690	1.8572
	25% Fe	**1.1065**	1.9895	**2.3286**	2.1237	**1.3749**	0.0822
	Fe free	1.5751	**2.7141**	3.4174	**3.6847**	3.5159	**2.9111**
125GPa	12.5% Fe	**1.4098**	**2.2438**	2.7630	2.8801	2.5944	1.9067
	25% Fe	**1.3362**	2.4883	**2.9335**	2.6718	**1.7033**	0.0278

Figure S1 Formation enthalpies of Mg-end member $MgSiO_3$ (orange line) and mixed phase $Mg_{0.875-x}Ca_{0.125}Fe_xSiO_3$ (blue line) as the function of iron.

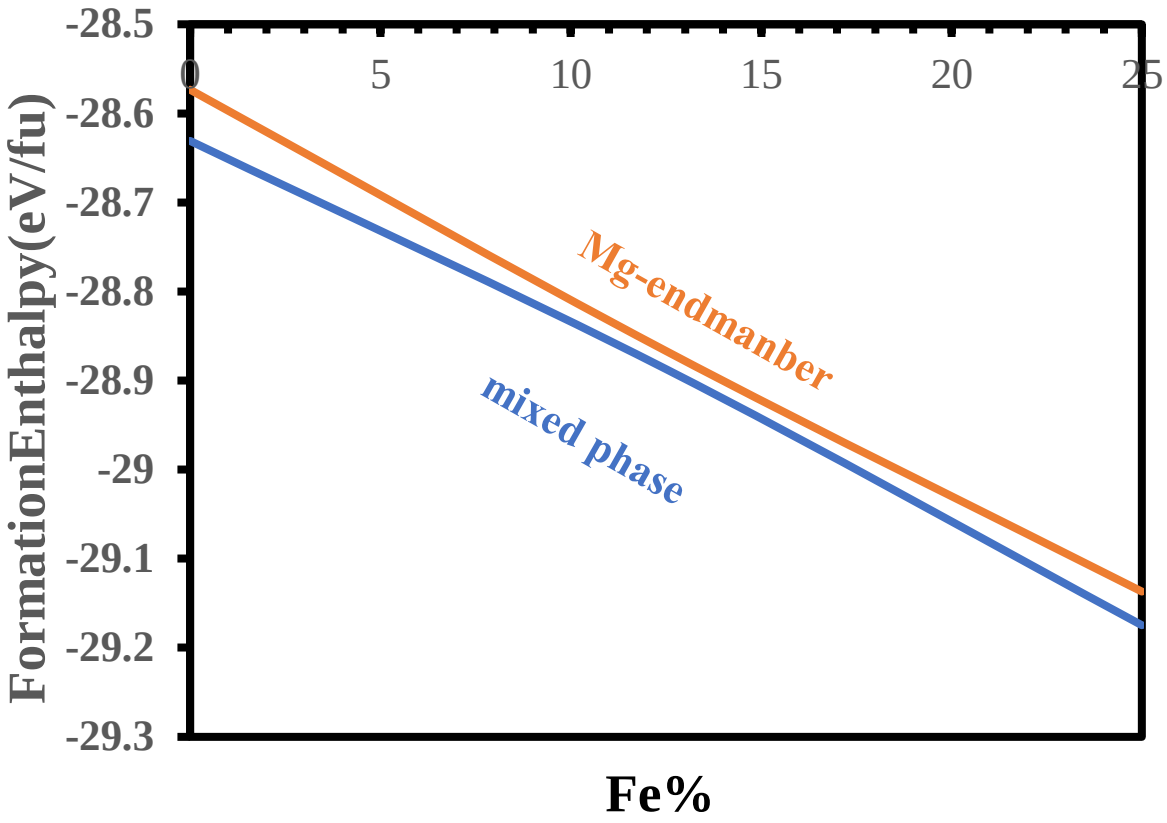

Figure S2 Plot of the mixing temperature (T_{mix}) for Ca: Mg =1:1 mixture of Ca-pv and Bridgmanite phases in Fe free (black line), 1% Fe (yellow line), 6.25% Fe (blue line) and 12.5% Fe (red line) bearing systems. The normal mantle geothermal gradient and the cold subduction slab geothermal is also presented for guidance(Ohtani et al. 2018)